



BIOMEDICAL SCIENCES

Long-term hepatic damage in high-fructose-fed C57BL/6 mice: hepatic fibrogenesis, endoplasmic reticulum stress markers, and fibrosis

BRENDA OLIVEIRA-CORDEIRO, ALINE FERNANDES-DA-SILVA, FLAVIA MARIA SILVA-VEIGA, CAROLLINE S. MIRANDA, FABIANE F. MARTINS & VANESSA SOUZA-MELLO

Abstract: The rising fructose intake in sugar-sweetened beverages and ultra-processed foods relates to the high incidence of nonalcoholic fatty liver disease. This study aimed to examine the effects of long-term high-fructose diet intake (for 16 or 20 weeks) on progressive hepatic damage, focusing on the endoplasmic reticulum stress markers and fibrogenesis as possible triggers of liver fibrosis. Forty 3-month-old male C57BL/6j mice were randomly divided into four nutritional groups: C16 (control diet for 16 weeks), C20 (control diet for 20 weeks), HFRU16 (high-fructose diet for 16 weeks), and HFRU20 (high-fructose diet for 20 weeks). Both HFRU groups showed oral glucose intolerance and insulin resistance, but only the HFRU20 group exhibited increased inflammation. The increased lipogenic and endoplasmic reticulum stress markers triggered hepatic fibrogenesis. Hence, time-dependent perivascular fibrosis with positive immunostaining for alpha-smooth muscle actin and reelin in HFRU mice was observed, ensuring fibrosis development in this mouse model. Our study showed time-dependent and progressive damage on hepatic cytoarchitecture, with maximization of hepatic steatosis without overweight in HFRU20 mice. ER stress and liver inflammation could mediate hepatic stellate cell activation and fibrogenesis, emerging as targets to prevent NAFLD progression and fibrosis onset in this dietary model.

Key words: fructose, NAFLD, hepatic fibrogenesis, ER stress, aging, hepatic stellate cell.

INTRODUCTION

The rising intake of fructose-rich foods is one of the main contributors to the high incidence of insulin resistance and hepatic steatosis worldwide (Jegatheesan & De Bandt 2017). Brazilians consume an average of 61 liters of sugar-sweetened beverages per year, linking increased fructose intake to the high incidence of cardiovascular, cerebrovascular, and metabolic diseases (BRASIL 2020). Glucose transporters (GLUT2 or GLUT5), which do not rely on insulin, mediate fructose absorption. The liver metabolizes the fructose excess, producing

glucose, triacylglycerols, non-esterified fatty acids (NEFA), and lactate, among others (Zhang et al. 2017), besides decreasing hepatic beta-oxidation while increasing hepatic lipogenesis (Lustig et al. 2012). This scenario results in triacylglycerol deposition within the hepatic parenchyma, the nonalcoholic fatty liver disease (NAFLD) (De Minicis et al. 2013), previously described in high-fructose-fed mice (Magliano et al. 2015).

Insulin resistance precedes NAFLD and causes endoplasmic reticulum (ER) stress, triggered by an imbalance between the unfolded proteins that enter the ER and the

cell's ability to process protein folding. If this imbalance persists, cell death is activated to protect the organism from the harmful effects of misfolded proteins (Hummasti & Hotamisligil 2010). Therefore, ER stress establishes a link between insulin resistance and inflammation. Proinflammatory signals stimulate hepatic stellate cell (HSC) differentiation into activated myofibroblast-like cells by fibrogenic gene activation (Yang et al. 2015).

In this context, non-alcoholic steatohepatitis (NASH) is becoming widespread and encompasses hepatic steatosis and hepatic inflammation with or without perisinusoidal fibrosis (Kazankov et al. 2019). HSC activation and macrophage (Kupffer cells) polarization are critical factors for the progression of liver fibrosis (Cao et al. 2022). Preclinical studies that evaluate NAFLD / NASH in a translational approach exhibit a wide range of diet composition and time of administration variation, compromising data comparison and reliable conclusions. Saturated fat and fructose overloads bear more resemblance to human NAFLD phenotype, but there is a lack of studies evaluating long-term exposure to these nutrients (Im et al. 2021). Clinical evidence has shown that high fructose intake correlates with increased liver fibrosis in adults, highlighting the hepatotoxicity of fructose (Abdelmalek et al. 2010). This study aimed to examine the effects of long-term high-fructose diet intake (for 16 or 20 weeks) on progressive hepatic damage, focusing on ER stress markers and fibrogenesis as possible triggers of liver fibrosis.

MATERIALS & METHODS

The study protocol, approved by the Ethical Committee in Animal Experimentation of the State University of Rio de Janeiro (CEUA 042/2018), followed the National Institutes of Health Guide

for the Care and Use of laboratory animals and Brazilian Federal Law nº 11.794/2008.

Animals and diet

Forty 3-month-old male C57BL/6J mice were group-housed in ventilated cages (n=5 per cage, Nexgen system, Allentown Inc., PA, USA) with controlled conditions of temperature ($21 \pm 2^\circ\text{C}$), humidity ($60 \pm 10\%$), and light (12:12h light-dark cycle), and unrestricted access to food and water. Animals were randomly divided into four nutritional groups (n=10 each):

- 1) C16 - fed the control diet (C) for 16 weeks (0% of energy as fructose; 15.88 kJ/g).
- 2) HFRU16 - fed a high-fructose diet (HFRU) for 16 weeks (50% of energy as fructose; 15.88 kJ/g).
- 3) C20 - fed the C diet for 20 weeks.
- 4) HFRU20 - fed an HFRU diet for 20 weeks.

The experimental diets produced by Prag Soluções (Jaú-SP, Brazil) followed the recommendations of the AIN-93M for rodents (Reeves et al. 1993). Supplementary Material - Table SI details the composition of the experimental diets. Based on a previous experiment that found evidence for HSC activation in this mouse strain after 17 weeks of the HFRU diet, we defined the two interruptions of the HFRU diet in this experiment (16 and 20 weeks) (Silva-Veiga et al. 2020).

Food intake, energy intake, and body mass (BM)

Food intake was obtained daily throughout the experimental protocol by subtracting the amounts of feed offered and feed not consumed after 24 h. Energy intake was the product of food intake and energy density per gram of each diet in kJ. Energy intake was also shown as kJ/100g BM/day to avoid bias due to different body masses. Animals' body masses were measured weekly.

Water intake and systolic blood pressure

Water intake was evaluated three times a week by subtracting the amount offered by the leftovers. Likewise, energy and water intake were shown as mL/100g BM/day. Systolic blood pressure was addressed in triplicate in conscious mice through non-invasive tail plethysmography (Insight, Ribeirão Preto, São Paulo, Brazil) at the end of the experiment. Mice got used to the method for two weeks before the official measurements.

Oral glucose tolerance test (OGTT)

In the week prior to euthanasia, mice fasted for 6 hours, and then a solution containing glucose (25% in sterile saline – 0.9% NaCl) at a dosage of 2g/kg body mass was administered by orogastric gavage. The animals' blood was obtained by milking the tail vein at time 0 and after glucose overload at times 15, 30, 60, and 120 minutes to check blood glucose levels using a glucometer (Accu-Chek, Roche, SP, Brazil). Baseline values were used as fasting glucose. The area under the curve (AUC) was calculated to address glucose tolerance (GraphPad Prism v 8.4.0, San Diego, CA, USA).

Euthanasia

In the sixteenth and twentieth weeks of the experimental protocol, animals from the respective groups were fasted for six hours and anesthetized with ketamine (240 mg/kg) and xylazine (30 mg/kg). Blood samples were obtained by cardiac puncture, centrifuged (712 xg, for 15 minutes), and frozen (-80°C) for further biochemical analysis. The liver was carefully dissected, weighed, and fixed in freshly prepared 4% w / v formaldehyde, 0.1 M phosphate buffer, pH 7.2 Millonig formalin (for light microscopy technique), or frozen (-80°C, for molecular analyses). The epididymal fat pad was dissected,

weighed, and expressed as a ratio of total body mass.

Biochemical analyses and FIRI

Plasma insulin and leptin concentrations were analyzed in duplicate with commercially available enzyme immunoassay kits (Rat/Mouse Insulin ELISA kit Cat. #EZRMI-13K) using the Fluostar Omega equipment (BMG LABTECH GmbH, Germany). Fasting glucose and insulin data were used to calculate the FIRI (Fasting Insulin Resistance Index) using the formula: $\text{fasting insulin (um/L)} \times \text{fasting glucose (mmol/L)} / 25$ (Duncan et al. 1995). Liver cholesterol and triacylglycerol concentrations were measured in frozen liver samples as described previously (Catta-Preta et al. 2011).

Light microscopy, stereology, and immunofluorescence

Liver fragments included in paraplast plus (Sigma-Aldrich, St. Louis, MO, USA) were cut (5 µm thickness) and stained with hematoxylin and eosin. Random fields were photographed using a light microscope (Olympus BX51, Olympus America Inc., Miami, USA) and a digital camera (Infinity 1-5 c, Lumenera Co., Ottawa, ON, Canada). The volume density (Vv) of hepatic steatosis was estimated using a 36-point test system defined by the STEPAnizer program (Tschanz et al. 2011) by the point counting technique (Catta-Preta et al. 2011). The Vv [steatosis] was estimated as follows: $Vv [st] = Pp [st, liver] / PT$, where Pp is the number of points that reach the fat droplets and PT is the total number of test points. Vv [steatosis] is considered an appropriate and reproducible stereological method to address liver steatosis compared to other methodologies currently used in rodents (Catta-Preta et al. 2011). Picrosirius red staining was performed to detect areas of liver fibrosis (Lattouf et al. 2014).

Regarding immunofluorescence, deparaffinized liver sections underwent antigen retrieval (citrate buffer, pH 6.0 at 60 °C for 20 min), followed by blockade with glycine 2% and the blocking buffer (PBS/BSA 5%), and incubation overnight at 4°C with the primary antibody (anti-alpha-smooth muscle actin, AB7817, or anti-reelin, AB78540, Abcam, Eugene, OR, USA), dilution 1:50 in PBS/BSA 1%. Then, the sections were incubated with the secondary antibody conjugated with the fluorochrome Alexa-546 for alpha-SMA and Alexa-488 for reelin (dilution 1:50 in PBS/BSA 1%) at room temperature for 1 hour. Slow Fade Antifade (Invitrogen, CA, USA) was used to mount the slides to keep fluorescence. The images were obtained using a confocal microscope (Nikon Confocal Laser Scanning Microscope, model C2, Nikon Instruments, Inc.).

RT-qPCR

A lysis solution (Trizol Invitrogen, CA, USA) extracted and isolated the total hepatic

mRNA. RNA concentration was determined by spectroscopy, using the Nanovue equipment (GE Life Sciences) and one μg of RNA and DNase I (Invitrogen). Oligo (dT) oligonucleotides for mRNA and Superscript III reverse transcriptase (Invitrogen, CA, USA) were used for cDNA synthesis. First-strand cDNA synthesis was performed using oligo (dT) primers for reverse transcriptase mRNA and Superscript III (both from Invitrogen). RT-qPCR was performed using a CFX96 recycler (Bio-Rad, Hercules, CA, USA) and SYBR Green mix (Invitrogen, Carlsbad, CA, USA). The mRNA relative expression ratio (QR) was calculated using the $2^{-\Delta\Delta\text{Ct}}$ equation, where ΔCt expressed the difference between the number of cycles (TC) of target genes and endogenous control. Table I describes sense and antisense primer sequences used for amplification.

Statistical analysis

Data were expressed as mean and standard deviation. Student T test with Welch correction

Table I. Forward and reverse sequences of RT-qPCR primers.

Primers	Forward	Reverse
Atf4	CCGAGATGAGCTTCTGAAC	ACCCATGAGGTTTCAAGTGC
Beta-actin	TGTTACCAACTGGGACGACA	GGGGTGTGAAGGTCTCAA
Chop	CTGCCTTTCACCTTGAGAC	CGTTTCTGGGGATGAGATA
Coll1a1	TAGGCCATTGTGTATGCAGC	ACATGTTTCAGCTTGTGGACC
Cidec	AGCTAGCCCTTCCAGAAG	TAGAGGGTTGCCTTCACGTT
Gadd45	GCGAGAACGACATCAACATC	GTTTCGTCACCAGCACACAGT
Smad3	GTCAACAAGTGGTGGCGTGTG	GCAGCAAAGGCTTCTGGGATAA
Srebp-1c	AGCAGCCCTAGAACAACA	TCTGCCTTGATGAAGTGTGG
Tgf-beta	ACTGGAGTTGTACGGCAGTG	GGCTGATCCCCTTGATTTCC
Yap-1	ACCCTCGTTTTGCCATGAAC	TGTGCTGGGATTGATATCCGTA
Ppar-gamma	ACGATCTGCCTGAGGTCTGT	CATCGAGGACATCCAAGACA
Alpha-sma	CCACCATGTACCCAGGCATT	GTGTGCTAGAGGCAGAGCAG

Abbreviations: Activating Transcription Factor 4 (*Atf4*), Beta-actin (constitutive gene), C/EBP homologous protein (*Chop*), Collagen Type I Alpha 1 Chain (*Col1a1*), cell death inducing DFFA like effector c (*Cidec*), Growth Arrest and DNA Damage (*Gadd45*), peroxisome proliferator-activated receptor-gamma (*Ppar-gamma*), SMAD Family Member 3 (*Smad3*), Sterol regulatory element-binding transcription factor 1 (*Srebp-1c*), transforming growth factor beta (*Tgf-beta*), Yes1 Associated Transcriptional Regulator (*Yap-1*), and alpha-smooth muscle actin (*Alpha-sma*).

was used to address differences between Control and HFRU groups regarding BM and energy intake weekly evolution (comparisons between two groups at the same time point). One-way analysis of variance (ANOVA) with Brown-Forsythe and Welch test and Dunnett T3 post-test was applied to test differences regarding biochemical, stereological, and molecular parameters (comparisons among four groups at different time points). These tests were chosen as homoscedasticity between groups was not assumed (Dunnett 1980). The two-way ANOVA was used to assess the influence of two variables – diet and time of diet administration – and their interaction on the evaluated parameters. The significance index was $p < 0.05$ in all cases (GraphPad Prism, version 8.4.0, CA, USA).

RESULTS

Excessive dietary fructose reduced body mass without altering the energy intake

All groups started the experiment with similar body masses (Figure 1a). From the 2nd until the 11th week, the HFRU group showed a smaller body mass than the C group. However, from the 12th to the 17th week, there was no difference regarding body mass between C and HFRU groups. From the 18th to the 20th week, the HFRU group showed a lower body mass than the C group (Figure 1a).

Energy intake showed as kJ/animal/day weekly (Figure 1b) or kJ/100g BM/day (Figure 1c) exhibited no difference between the groups since the diets are isoenergetic (Table SI).

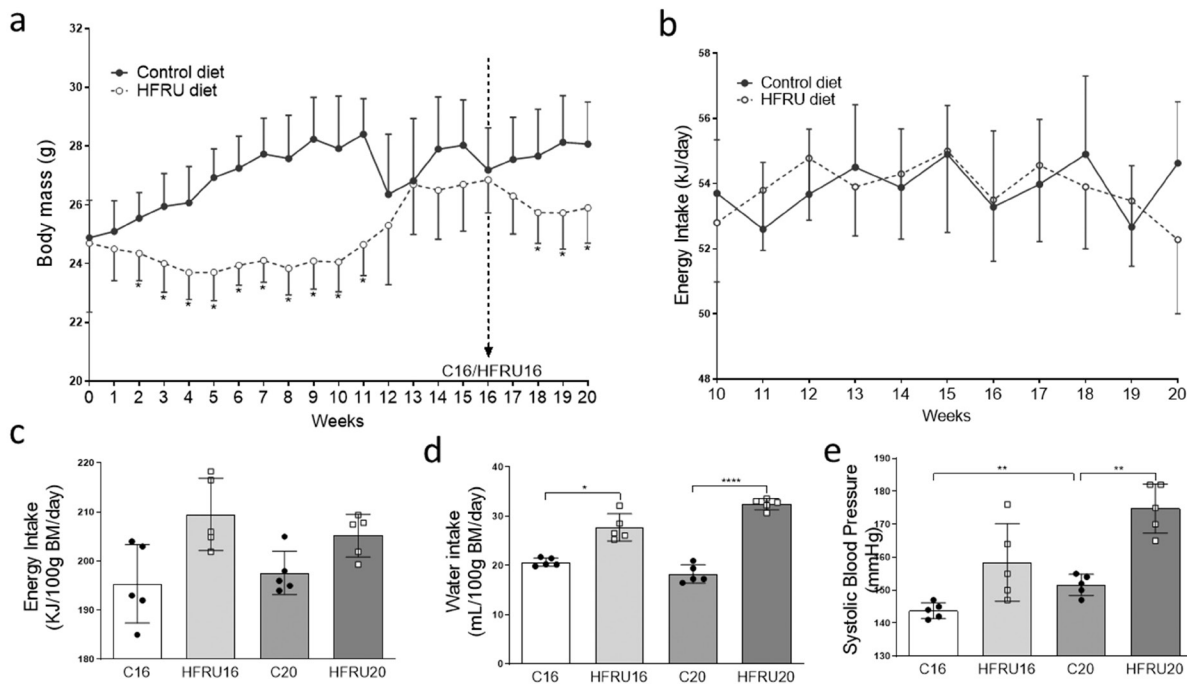


Figure 1. Body mass evolution for 20 weeks (a), energy intake from weeks 10 to 20 (b), energy intake - kJ/100g body mass (c), water intake – mL/100g body mass (d), systolic blood pressure (e). Student T test and Welch correction (mean ± SD, n=5) tested the differences between C and HFRU (* P<0.05) in Figures a, and b. Welch and Brown-Forsythe one-way ANOVA and Dunnett t3 post hoc test (mean ± SD, n=5) tested the differences are indicated: * P<0.05, ** P<0.01, and **** P<0.0001. Each dark circle represents a C animal, and each white square represents an HFRU animal. Abbreviations: C (Control diet), HFRU (High-fructose diet).

Fructose intake increased water intake and systolic blood pressure

Water intake/100g BM/day increased in fructose-fed groups independent of age (Figure 1d). Conversely, fructose intake increased systolic blood pressure only in the HFRU20 animals. Aging also influenced systolic blood pressure, as the C20 mice had higher pressure levels than the C16 mice (Figure 1e).

Chronicity of the HFRU diet disrupted the adiposular axis

Figure 2a shows the OGTT curve. The AUC analysis revealed a significant increase in the HFRU16 and HFRU20 groups compared to their age-matched counterparts. However, the HFRU20 group had a lower AUC than the HFRU16 (Figure 2b). In line with the OGTT data, HFRU16 and HFRU20 groups had hyperinsulinemia (Figure 2c) and, hence, FIRI confirmed insulin resistance at both times of administration of the HFRU diet (Figure 2d).

The epididymal fat/body mass ratio was lower in the HFRU16 group than in the C16 group. Conversely, the HFRU20 group increased the epididymal fat/body mass ratio (Figure 3a). In Figure 3b, plasma leptin concentrations followed the epididymal fat data, with increased levels only in the HFRU20 group compared to the C20 group.

The HFRU diet elicited a time-dependent maximization of hepatic steatosis

Liver mass/body mass ratio augmented in the HFRU groups compared to their age-matched C groups, with a time-dependent increase between HFRU16 and HFRU20 groups (Figure 3c). As for hepatic cholesterol, only the HFRU20 group had higher values than the C20 group, but there was a time-dependent increment in hepatic cholesterol concentrations between the HFRU groups (Figure 3d).

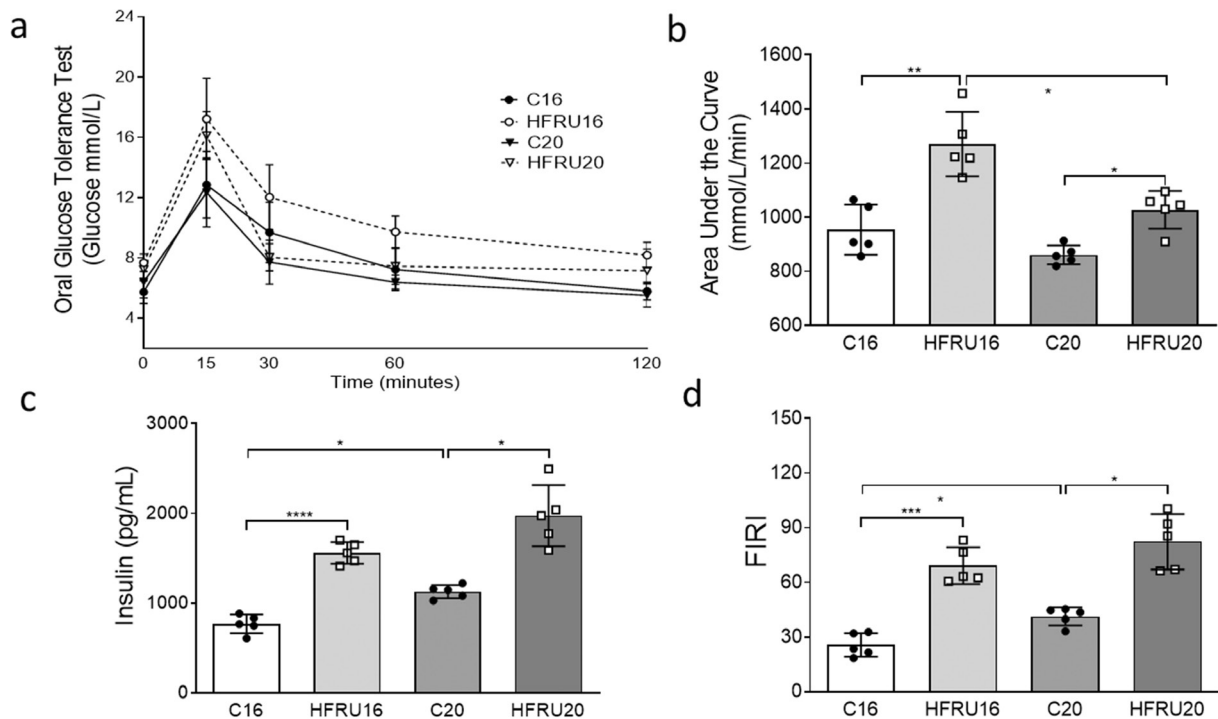


Figure 2. Oral Glucose Tolerance Test (a), Area under the curve (b), Plasma insulin (c), and FIRI (d). Welch and Brown-Forsythe one-way ANOVA and Dunnett t3 post hoc test (mean ± SD, n=5). Differences are indicated: * P<0.05; ** P<0.01; *** P<0.001; and **** P<0.0001. Each dark circle represents a C animal, and each white square represents an HFRU animal. Abbreviations: C (Control diet), HFRU (High-fructose diet); Fasting insulin resistance index (FIRI).

Chronic fructose consumption enhanced lipid deposition in the livers of the HFRU groups, as shown in Figure 4a. The HFRU16 group had a predominance of macrovesicular steatosis, whereas the HFRU20 group showed macrovesicular steatosis coupled with increased microvesicular steatosis. The control groups showed preserved liver parenchyma, but the C20 group showed an increase in the space of Disse, which may be related to the aging process.

Stereology confirmed that both HFRU16 and HFRU20 groups had higher Vv [steatosis] than their counterparts (Figure 4b). Interestingly, there was maximization of hepatic steatosis with the chronic HFRU diet intake, with a 94% increase in the Vv [steatosis] in the HFRU20 compared to the HFRU16. Likewise, hepatic triacylglycerol concentrations showed a 160% increment in the HFRU20 group compared to the HFRU16 (Figure 4c).

Chronic HFRU intake increased lipotoxicity, inflammation, and ER stress markers

The lipogenic transcription factor *Ppar-gamma* showed increased gene expression in both HFRU groups (Figure 5a). The lipogenic gene *Srebp-1c* (*Ppar-gamma* transcript) was upregulated in the HFRU20 group compared to the C20 group (Figure 5b), whereas *Cidec* (*Srebp-1c* transcript) showed higher expression in both HFRU groups than in their age-matched C groups (Figure 5c).

The oral glucose intolerance and enhanced hepatic lipogenesis upregulated genes related to ER stress: *Atf4* augmented both in HFRU16 and HFRU20 groups (Figure 5d), while its downstream gene *Chop* showed an 849% increase in the HFRU20 group (Figure 5e). Lastly, *Gadd45* was higher in both groups that consumed the HFRU diet than in their age-matched C groups (Figure 5f).

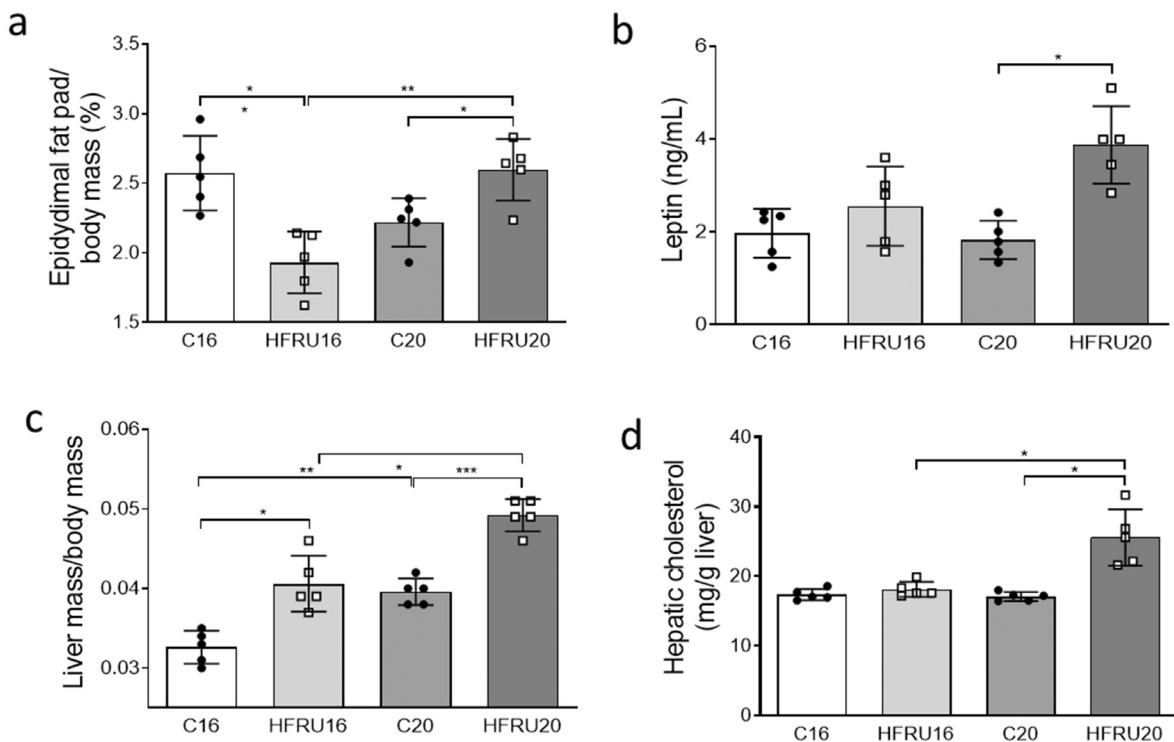


Figure 3. Epididymal fat pad/body mass (a), Plasma leptin (b), Liver mass/body mass (c), and Hepatic cholesterol concentrations (d). Welch and Brown-Forsythe one-way ANOVA and Dunnett t3 post hoc test (mean \pm SD, n=5). Differences are indicated: * $P < 0.05$; ** $P < 0.01$; and *** $P < 0.001$. Each dark circle represents a C animal, and each white square represents an HFRU animal. Abbreviations: C (Control diet), HFRU (High-fructose diet).

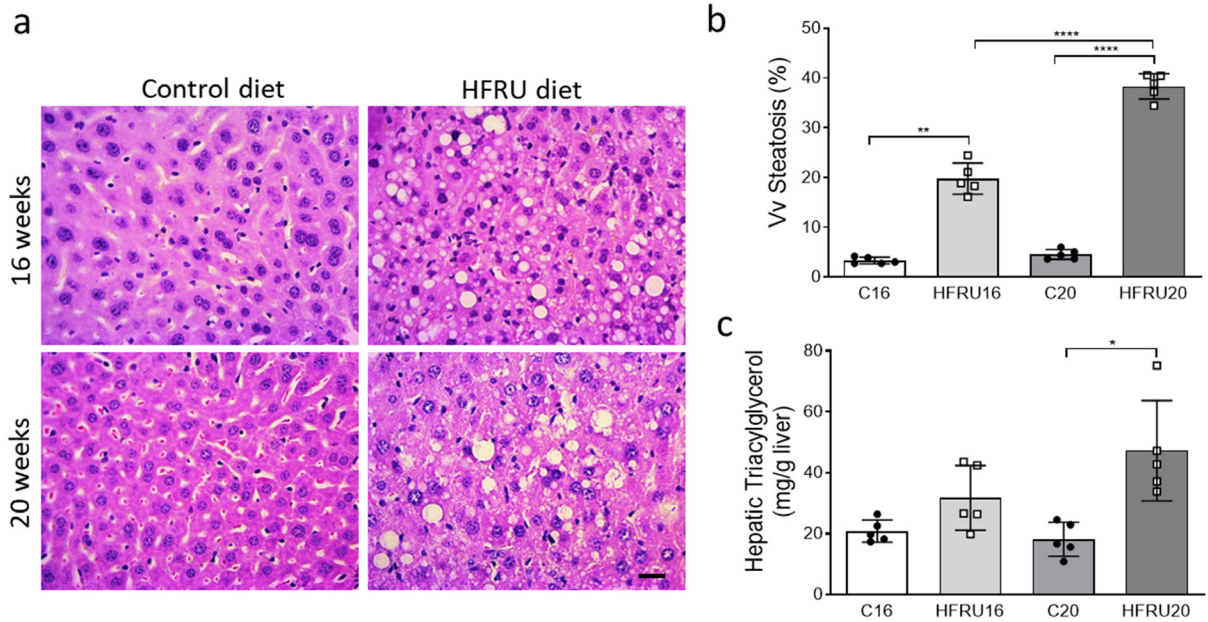


Figure 4. Liver histology (a), Volume density of hepatic steatosis (b), and Hepatic triacylglycerol concentrations (c). Photomicrographs show normal hepatic parenchyma in the C16 and C20 groups, a predominance of macrovesicular steatosis in the HFRU16 group, and marked microvesicular and macrovesicular steatosis in the HFRU20 group (scale bar = 40µm). Welch and Brown-Forsythe one-way ANOVA and Dunnett t3 post hoc test (mean ± SD, n=5). Differences are indicated: * P<0.05; ** P<0.01; and **** P<0.0001. Each dark circle represents a C animal, and each white square represents an HFRU animal. Abbreviations: C (Control diet), HFRU (High-fructose diet), Vv (volume density).

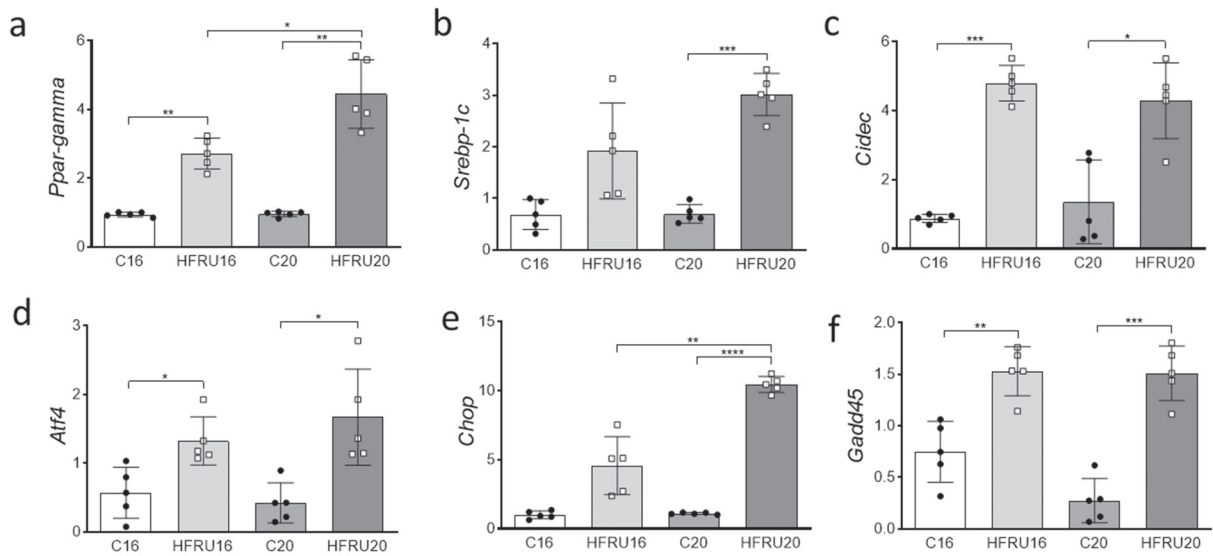


Figure 5. Liver gene expression of *Ppar-gamma* (a), *Srebp-1c* (b), *Cidec* (c), *Atf4* (d), *Chop* (e), and *Gadd45* (f). Welch and Brown-Forsythe one-way ANOVA and Dunnett t3 post hoc test (mean ± SD, n=5). Differences are indicated: * P<0.05; ** P<0.01; *** P<0.001; and **** P<0.0001. Each dark circle represents a C animal, and each white square represents an HFRU animal. Abbreviations: C (Control diet), HFRU (High-fructose diet), *Ppar-gamma* (peroxisome proliferator-activated receptor-gamma), *Srebp-1c* (Sterol regulatory element-binding protein), *Cidec* (Cell Death Inducing DFFA Like Effector C), *Atf4* (Activating Transcription Factor 4), *Chop* (C/EBP homologous protein), *Gadd45* (Growth Arrest and DNA Damage 45).

The HFRU diet elicited hepatic stellate cell activation, fibrogenesis, and fibrosis maximization in the long term

The high fructose intake significantly augmented the expression of genes related to HSC activation: *Tgf-beta1* (Figure 6a), *Smad3* (Figure 6b), and their transcript *Col1a1* (Figure 6c) were significantly higher in both HFRU groups than in their counterparts. Moreover, *Yap-1* (linked to NAFLD transition into NASH, Figure 6d) showed a 131% increase in the HFRU16 group and a 265% increase in the HFRU20 group compared to age-matched C groups.

To further confirm the activation of HSC, the photomicrographs of Figure 6e show a marked collagen deposition in the HFRU20 group, followed by the HFRU16 group, suggesting a more pronounced accumulation of extracellular matrix proteins because of HSC activation. In line with these observations, the alpha-SMA protein (Figure 7a, red labeling) and gene expression (Figure 7b) showed a significant

increase in the HFRU20 group compared to the C20 group. Furthermore, the HFRU20 group also showed positive immunostaining for reelin (Figure 7a, green labeling), a specific marker for HSC activation, in contrast to negative immunoreaction for reelin in the C20 group (Figure 7c).

Two-way ANOVA results

Diet was the factor that exerted the most significant influence in determining the parameters: body mass, water intake, systolic blood pressure, AUC for OGTT, blood glucose, insulin, FIRI, leptin, hepatic triacylglycerol, hepatic cholesterol, Vv [steatosis], gene expression of lipogenic (*Ppar-gamma*, *Srebp-1c*, and *Cidec*), ER stress (*Atf4*, *Chop*, and *Gadd45*), and HSC activation (*Alpha-sma*, *Tgf-beta1*, *Smad3*, *Col1a1*, and *Yap-1*) markers.

The duration of diet administration (time) was the factor that most influenced the liver mass. There was a significant interaction between

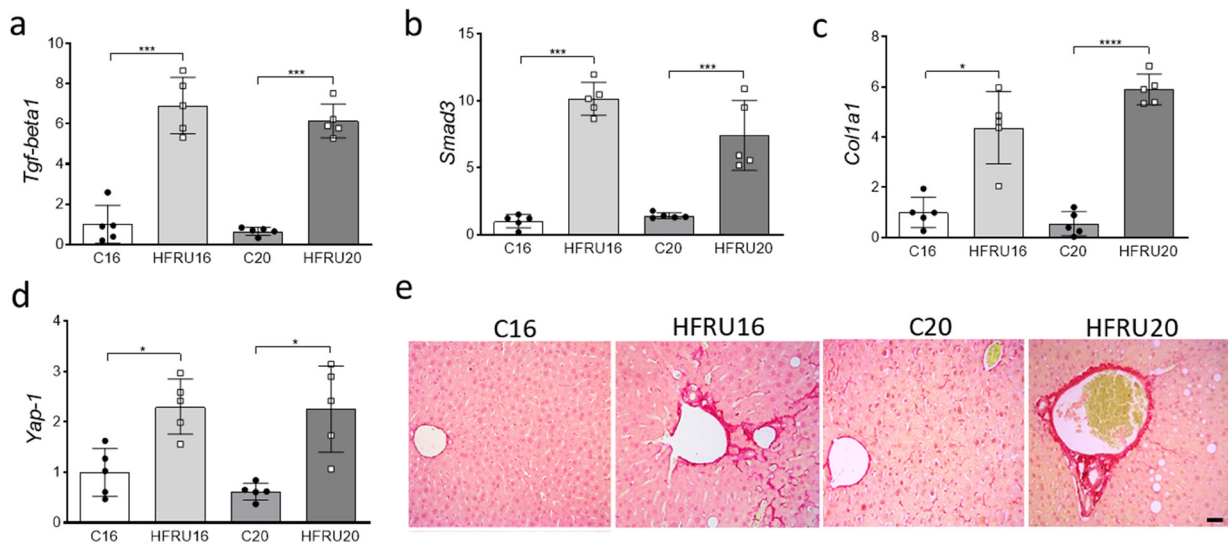


Figure 6. Liver gene expression of *Tgf-beta1* (a), *Smad3* (b), *Col1a1* (c), *Yap-1* (d), Picrosirius red staining (e). a-d: Welch and Brown-Forsythe one-way ANOVA and Dunnett t3 post hoc test (mean ± SD, n=5). Differences (P<0.05) are indicated: * P<0.05; *** P<0.001; and **** P<0.0001. Each dark circle represents a C animal, and each white square represents an HFRU animal. e: Photomicrographs show noticeable perivascular collagen deposition in livers from HFRU mice, with exacerbation in the HFRU20 group, scale bar = 10µm. Abbreviations: C (Control diet), HFRU (High-fructose diet), *Tgf-beta1* (Transforming growth factor-beta 1), *Smad3* (SMAD Family Member 3), *Col1a1* (Collagen Type I Alpha 1 Chain), *Yap-1* (Yes1 Associated Transcriptional Regulator).

diet and time on the parameters: body mass, water intake, epididymal fat, leptin, hepatic cholesterol, Vv [steatosis], and the expression of the following genes: *Ppar-gamma*, *Srebp-1c*, *Chop*, *Smad3*, and *Col1a1*. The two-way ANOVA results are detailed in Table II.

DISCUSSION

The present results showed that chronic fructose intake in C57BL/6J mice caused systolic hypertension, oral glucose intolerance, and increased intra-abdominal fat percentage without being overweight. These metabolic impairments are predictors of hepatic steatosis, verified after 16 weeks and intensified after 20 weeks of HFRU diet intake. Hyperinsulinemia increased ER stress markers, hepatic lipogenesis, and liver inflammation, triggering HSC activation. Hence, increased fibrogenesis was observed in the livers of HFRU-fed mice, resulting in time-dependent perivascular liver fibrosis, indicating

a possible progression from NAFLD to NASH between 16 and 20 weeks of HFRU diet intake.

Control and HFRU groups maintained similar body masses from the 12th until the 17th weeks (when most experiments are interrupted). However, from the 18th to the 20th week, the HFRU group showed a reduced body mass. Previously, our group showed that HFRU diet feeding for 20 weeks led to reduced body mass with great adiposity (de Oliveira Sa et al. 2017), and the increased obligatory thermogenesis after fructose intake in comparison with the same amount of glucose might explain this effect of the long-term fructose intake (for five months) (Tappy & Jequier 1993). Conversely, a 12-week or 16-week high-fructose diet protocol yielded expressive hepatic steatosis without changing body mass in C57BL/6 mice (Do et al. 2018, Silva-Veiga et al. 2020), agreeing with the present results regarding the HFRU16 group. Liver fibrosis might mediate the reduction of body mass between 18 and 20 weeks of the HFRU diet once cancer-cachexia in mice is associated

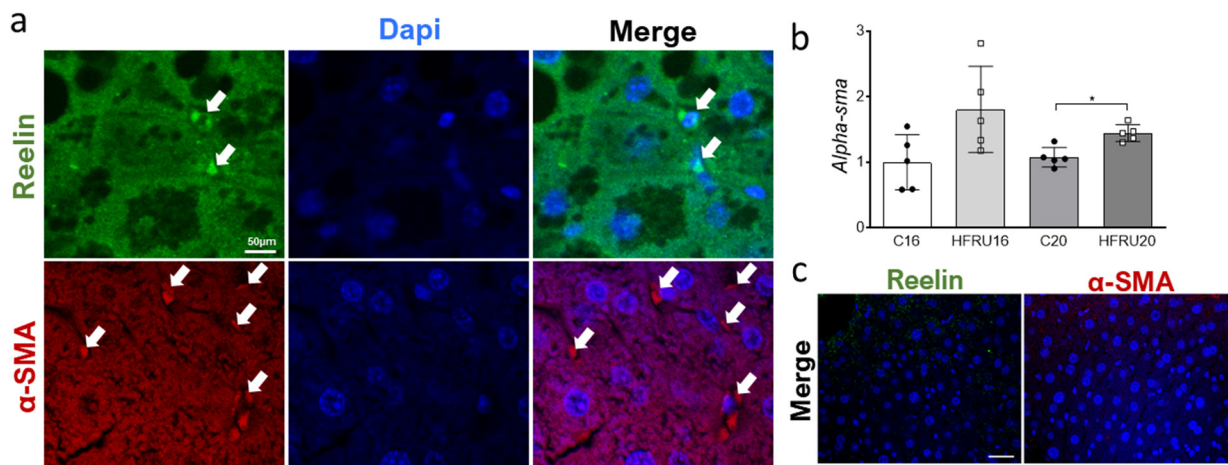


Figure 7. Immunofluorescence for Reelin, and α -SMA in HFRU20 group (a), liver gene expression of *Alpha-sma* (b), immunofluorescence for Reelin, and α -SMA in C group (c). a: Confocal microscopy showing positive immunofluorescence for alpha-smooth muscle actin (red labeling) and reelin (green labeling) at the space of Disse in livers from HFRU20, scale bar = 10 μ m. This result confirms the activation of the hepatic stellate cell. b: Welch and Brown-Forsythe one-way ANOVA and Dunnett t3 post hoc test (mean \pm SD, n=5). The difference is indicated: * P<0.05. Each dark circle represents a C animal, and each white square represents an HFRU animal. c: Negative immunoreactions for alpha-smooth muscle actin and reelin in the C20 group. Abbreviations: C (Control diet), HFRU (High-fructose diet), *Alpha-sma* (alpha-smooth muscle actin).

with liver fibrosis through enhanced collagen deposition, protein turnover, and mitochondrial quality control (Rosa-Caldwell et al. 2020).

The increased water intake in high-fructose-fed mice occurs due to diet palatability, and the consequent hypervolemia causes systolic

hypertension in the long run, as previously documented in this mouse strain using the same HFRU diet (Silva-Veiga et al. 2020, Camelo et al. 2019). Interestingly, the C20 group showed higher systolic blood pressure than the C16 group. A previous study confirmed an age-dependent

Table II. Detailed two-way ANOVA results.

Parameters	Interaction		Time of diet administration		Diet	
	% total variance	P value	% total variance	P value	% total variance	P value
Energy intake	6.221	NS	0.000	NS	3.414	NS
Water intake	6.251	0.0103	0.025	NS	81.90	<0.0001
Final body mass	8.076	0.0421	20.58	0.0028	44.86	<0.0001
Liver mass/body mass	0.406	NS	38.56	<0.0001	49.08	<0.0001
Hepatic cholesterol	23.24	0.0011	20.11	0.0019	33.28	0.0002
Hepatic triacylglycerol	9.515	NS	4.693	NS	46.22	0.0005
Epididymal fat pad %	52.32	<0.0001	28.19	0.0001	1.977	NS
AUC OGTT	4.818	NS	24.35	0.0004	50.79	<0.0001
Vv steatosis	4.374	0.0010	8.266	<0.0001	83.05	<0.0001
Leptin	13.09	0.0290	8.455	NS	42.04	0.0006
Blood glucose	7.591	NS	0.319	NS	46.00	0.0010
Systolic blood pressure	2.679	NS	21.22	0.0018	51.76	<0.0001
Insulin	0.085	NS	16.01	0.0003	71.38	<0.0001
FIRI	0.075	NS	8.938	0.0054	77.19	<0.0001
Gene expression						
Srebp-1c	6.287	0.0381	6.559	0.0346	67.48	<0.0001
Cidec	1.715	NS	0.001	NS	81.74	<0.0001
Ppar-gamma	7.819	0.0031	8.128	0.0026	73.76	<0.0001
Alpha-sma	5.177	NS	2.218	NS	36.98	0.0049
Atf4	3.494	NS	0.555	NS	57.60	0.0002
Chop	13.32	<0.0001	14.27	<0.0001	66.27	<0.0001
Gadd45	3.828	NS	4.534	0.0462	76.11	<0.0001
Tgf-beta1	0.123	NS	0.874	NS	90.94	<0.0001
Smad3	3.650	0.0288	1.998	NS	84.23	<0.0001
Col1a1	4.277	0.0223	1.291	NS	83.74	<0.0001
Yap-1	0.835	NS	1.444	NS	66.19	<0.0001

The most potent factor influencing the total variance for each parameter appears in bold, and NS stands for non-significant influence. Abbreviations: Area under the curve (AUC), Oral glucose tolerance test (OGTT), Volume density (Vv), Fasting insulin resistance index (FIRI), Activating Transcription Factor 4 (*Atf4*), C/EBP homologous protein (*Chop*), Collagen Type I Alpha 1 Chain (*Col1a1*), cell death inducing DFFA like effector c (*Cidec*), Growth Arrest and DNA Damage (*Gadd45*), peroxisome proliferator-activated receptor (PPAR), SMAD Family Member 3 (*Smad3*), Sterol regulatory element-binding transcription factor 1 (*Srebp-1c*), transforming growth factor beta (*Tgf-beta*), Yes1 Associated Transcriptional Regulator (*Yap-1*), and alpha-smooth muscle actin (*Alpha-sma*).

increase in systolic blood pressure in C57BL/6 mice due to increased vascular tone after 28 weeks of age (the C20 group was 32 weeks old) (Wirth et al. 2016).

Regarding carbohydrate metabolism, the HFRU diet disrupts glucose homeostasis, contributing to insulin resistance, inflammation, and impaired hepatic beta-oxidation while favoring hepatic lipogenesis (Koo 2013, Silva-Veiga et al. 2020). Although excessive dietary fructose promoted oral glucose intolerance in both HFRU groups, the HFRU20 showed a lower AUC than the HFRU16, suggesting senescence of the pancreatic islets with the chronicity of the HFRU diet. These findings agree with a recent study, where high fat/high fructose (HF/HFRU) feeding for 12 weeks caused islet hypertrophy and hyperinsulinemia in rats, but continuing HF/HFRU feeding for 18 months caused decreased islet size and insulin immunostaining (Zhao et al. 2022). Our results suggest that islet exhaustion may begin between 16 and 20 weeks of HFRU diet intake in C57BL/6J mice.

In line with the OGTT data, the HFRU groups had hyperinsulinemia and insulin resistance. Of note, insulin levels were higher in the C20 than in the C16 group, agreeing with a previous study that showed that islets from aging mice exhibit an enhanced basal insulin secretion compared to adolescent mice (Avrahami et al. 2015). Changes in visceral fat depots and leptin concentrations were time dependent. The HFRU20 group had a disrupted adipoinular axis, with an augmented epididymal fat pad and the consequent hyperleptinemia, eliciting hyperinsulinemia (Kieffer & Habener 2000). It can be argued that HFRU20 animals had visceral white adipocyte hypertrophy, as previously shown in mice fed the same HFRU diet for 11 weeks (Magliano et al. 2015). These results comply with lipotoxicity, where surplus dietary fat cannot be stored in the enlarged adipocytes

and diverts to non-adipose sites such as the liver (Gustafson & Smith 2015).

Ectopic liver fat accumulation causes intracellular organelles to increase, eliciting increased liver mass/body mass ratio, besides a high Vv [steatosis] in both HFRU groups (Pais et al. 2013, Kim et al. 2015). Even though the C20 group did not show higher Vv [steatosis] than the C16 group, this group showed an augmented liver mass/body mass ratio. In agreement, the liver mass shows a 1.3-fold increase in 19 months-old compared to 3 months-old mice (Stahl et al. 2020). In the HFRU groups, the increased lipid deposition in the liver correlated to augmented hepatic triacylglycerols (Catta-Preta et al. 2011), regardless of age. Insulin resistance favors lipolysis in the white adipose tissue, with a substantial NEFA influx to the liver (Pais et al. 2013). In contrast, insulin resistance reduces the liver's capacity to metabolize the high NEFA influx, resulting in hepatic triacylglycerol deposition and increased low-density lipoprotein (Asgharpour et al. 2016). A previous study from our group characterized NAFLD with significantly increased Vv [steatosis] and alanine aminotransferase after an 11-week dietary protocol using the same HFRU diet and mice strain (Magliano et al. 2015). Herein, we observed a maximization of liver steatosis from the 16th to the 20th week of excessive dietary fructose intake.

Diets high in simple sugars (>20% kcal) can result in elevated hepatic triacylglycerols due to the upregulation of transcription factors that induce *de novo* lipogenesis (DNL) in mice (Vasques-Monteiro et al. 2021). However, a four-week high-fructose diet (60% w/w) intake in pigs upregulated DNL genes in the liver, but not to the same extent as it increased in their adipose tissue, failing to develop NAFLD as in rodents and humans (Schmidt et al. 2021). Hepatic DNL relies on insulin, which activates

the sterol regulatory element-binding protein 1c (SREBP-1c) maturation initially in the ER (Herman and Samuel 2016, Ferre and Fofelle 2010). The high insulin concentrations triggered increased *Srebp-1c* and the maximization of hepatic steatosis in the HFRU20 group. Likewise, cell death-inducing DFFA-like effector c (*Cidec*), related to the size of lipid inclusion within the hepatocyte, was upregulated in both HFRU groups and agreed with the high hepatic triacylglycerol concentrations in the HFRU20 group (Aibara et al. 2020, Ito et al. 2010).

The HFRU20 animals had high liver cholesterol concentrations, a predictor of liver inflammation (Wouters et al. 2008). In this context, the increased plasma leptin concentrations in the HFRU group confirm this assumption of a pro-inflammatory state in these animals once hyperleptinemia and leptin resistance correlates to fatty liver (Lanaspa et al. 2018). These results suggest a maximization of hepatic damage in the HFRU20, confirmed by the interaction between diet x time of administration by the two-way ANOVA regarding the Vv [liver steatosis]. In agreement with these observations, high fructose intake has recently maximized hepatic steatosis in ovariectomized female mice through upregulation of tumor necrosis factor- α , macrophage infiltration, and HSC activation after 12 weeks of dietary protocol. Inflammation was not detected in ovariectomized female mice fed with a control diet, highlighting fructose as a potential trigger of NAFLD progression through pro-inflammatory signals (Ohashi et al. 2018).

Impaired glucose homeostasis, lipotoxic, and pro-inflammatory signals converge to trigger ER stress. ER comprises a continuous membrane system with different domains: sheet and tubule structures with bound ribosomes, rough endoplasmic reticulum, or without ribosomes, smooth endoplasmic reticulum (Shibata et al.

2006). Under stress, an adaptive response, the unfolded protein response (UPR), is activated to restore the ER lumen homeostasis. Chronic ER stress and defective UPR signaling are surrogates for lipotoxicity in the peripheral tissues (Han & Kaufman 2016). In this context, out of the three main UPR branches, the activating transcription factor 4 (*Atf4*), upregulated in both HFRU-fed groups, regulates lipid metabolism in response to nutritional stimuli. Hence, *Atf4* stimulates hepatic lipogenesis through *Srebp-1c* and maximizes hepatic steatosis (Xiao et al. 2013). *Atf4* ablation in mice with alcohol-induced hepatic mitochondrial dysfunction improved mitochondrial biogenesis and respiration owing to mitochondrial transcription factor A (TFAM) restoration (Hao et al. 2021). The upregulation of *Atf4* and its downstream gene *Chop* in the HFRU20 group explains the 1-fold increase in Vv [steatosis] in the HFRU20 compared to the HFRU16 group and implies mitochondrial damage in long-term HFRU feeding in this mouse model.

This study showed that *Atf4* enhanced its downstream gene C/EBP homologous protein (*Chop*) in the HFRU20 group. *Chop* is a critical marker of hepatic injury because it links ER stress to hepatic inflammation and lipotoxicity through lipogenic and adipogenic stimuli (Wang et al. 2013, Rutkowski et al. 2008). Moreover, *Chop* is a potent inducer of apoptosis as it disrupts the cell cycle, resulting in cell death (Fusakio et al. 2016, Fernandes-da-Silva et al. 2021).

Apoptosis aims to protect hepatocytes from the harmful effects triggered by the action of unfolded proteins (Galligan et al. 2012, Fusakio et al. 2016). Likewise, the growth arrest and DNA damage (*Gadd45*) exhibited a high expression in both HFRU groups, indicating increased damage through diminished cellular proliferation and favored cell death (Oyadomari & Mori 2004, Tian & Locker 2013). In this context, a recent study

showed that old aged C57BL/6 mice (24 months old) fed a control diet develop initial liver fibrosis secondary to liver inflammation, present signs of hepatocyte senescence (increased PAI-1 expression), and increased apoptosis (increased caspase-3 expression). Inflammatory pathways such as bacterial endotoxin and toll-like receptor-4 activation mediated these findings in aging mice (Jin et al. 2020). In the present study, fructose may anticipate inflammation-driven liver fibrosis, observed in the HFRU20 mice that were eight months old.

The progressive fructose-driven hepatic damage involved HSC activation and increased fibrogenesis, indicating NAFLD progression toward NASH. In this context, the Yes1-associated transcriptional regulator (*Yap-1*) is an early and pivotal regulator of HSC activation, promoting scarring during NASH. Our results showed upregulated *Yap-1* coupled with a high percentage of hepatic steatosis and increased alpha-smooth muscle actin (*Alpha-sma*, a myofibroblast marker) expression in the HFRU20 group, reinforcing the suggested transition from NAFLD to NASH in this HFRU-fed mouse model (Mannaerts et al. 2015, Machado et al. 2015). A previous study of our group showed a direct relationship between the activation of pro-fibrogenic genes with elevated expression of myofibroblast markers and activated HSC in the liver of ob/ob mice (Martins et al. 2021), implying that the present dietary protocol can cause similar harm to the liver.

Concerning the role of pro-fibrogenic markers in HSC activation, the transforming growth factor-beta 1 (*Tgf-beta1*) is considered the most potent fibrogenic cytokine, which binds and phosphorylates the type I receptor triggering SMAD family member 3 (SMAD3) (Hellerbrand et al. 1999). Activation of SMAD3 stimulates HSC, promoting the transcription of type I and III collagen (Breitkopf et al. 2006, Friedman 2008),

causing liver fibrosis. *Tgf-beta*, *Smad3*, and collagen type I alpha 1 chain (*Col1a1*) increased in the HFRU groups, characterizing an excessive deposition of extracellular matrix elements produced by activated HSC (Sferra et al. 2017).

The Picrosirius staining method, selective for connective tissue, allows the qualitative assessment of collagen fiber deposition (Kannt et al. 2020). In the fibrotic liver, type I and III collagen are the most abundant extracellular matrix components (Smith-Cortinez et al. 2021). Activated HSCs migrate and accumulate at tissue repair sites, secreting large amounts of extracellular matrix, mainly type I collagen, and regulating extracellular matrix remodeling (Urtasun et al. 2012). In the present study, the HFRU groups showed perivascular collagen deposition, an early sign of liver fibrosis (George et al. 2001), which became more pronounced after 20 weeks of HFRU feeding.

The same animals with maximized collagen deposition showed positive labeling for α -SMA at the space of Disse, confirming the presence of activated HSC after 20 weeks of HFRU feeding in this mouse model (Friedman 2008). Reelin, a marker for activated HSC in hepatotoxic fibrosis mice model (CCL4), also showed positive immunoreactions in the HFRU20 group, confirming the activation of a subset of this fibrogenic cell (Chen et al. 2022, Lua et al. 2016). This scenario suggests the accumulation of extracellular matrix proteins and perivascular fibrosis due to the stimuli of profibrogenic genes under ER stress and inflammation in the liver and the resulting HSC activation by chronic excessive fructose intake. Of note, at this stage (featuring cell stress and liver inflammation), hepatic fibrosis is irreversible. Then, a nutritional trigger can drive end-stage liver disease in the long term (Jegatheesan & De Bandt 2017, Lim et al. 2010).

Of note, the Taconic mice model of NASH used a diet comprised of 40% of energy as fat, 20% of energy as fructose, and 2% of energy as cholesterol to induce substantial hepatic inflammation after 16 weeks of the dietary protocol and fibrosis after 26 weeks of feeding (Radhakrishnan et al. 2021). Our model used 50% of energy as fructose in the HFRU diet. This fructose overload seems to anticipate the occurrence of hepatic inflammation and fibrosis to the 20th week of the dietary protocol. Figure 8 summarizes the main findings of the present study.

This study has some limitations as we could not evaluate female mice and two branches of the UPR due to restrictions imposed by the pandemic (limited access to the laboratory and PCR thermocycler, lent for COVID-19 diagnosis). Also, expansion of this dietary protocol (for 24 or 28 weeks) could maximize the outcomes observed herein and provide new insights into

liver fibrosis driven by nutritional imbalances in mice.

In conclusion, excessive dietary fructose caused ectopic accumulation of lipids in the hepatic parenchyma after 16 and 20 weeks of diet administration in C57BL/6J mice, with time-dependent maximization of hepatic steatosis, without overweight. Hepatic ER stress markers, lipogenesis, and inflammation were surrogates for the upregulation of profibrogenic genes and HSC activation, resulting in time-dependent perivascular fibrosis in the liver of HFRU animals. These results suggest that the intake of 50% of energy as fructose for 20 weeks promoted liver inflammation, HSC activation, and perivascular fibrosis, characterizing the transition from NAFLD to NASH in C57BL/6J mice. Dietitians and hepatologists should discourage excessive fructose intake due to progressive deleterious effects on the liver.

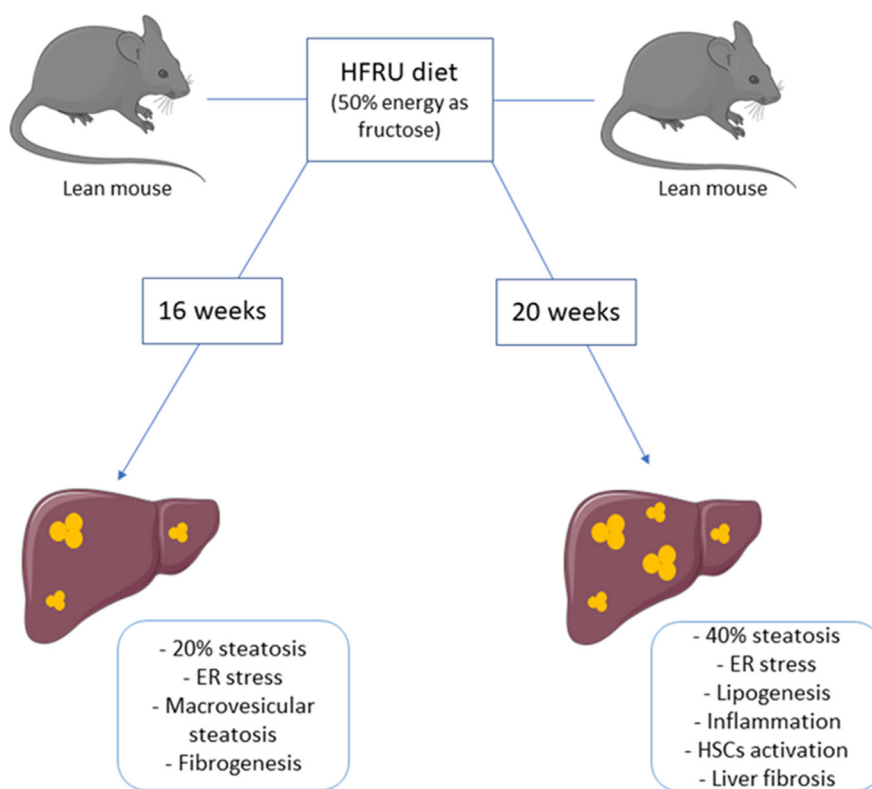


Figure 8. Summary of the main results. Lean mice consumed a high-fructose diet (HFRU, 50% of energy as fructose) for 16 or 20 weeks. HFRU16 mice remained lean and showed 20% Vv [steatosis], secondary to increased lipogenesis and increased ER stress markers. This scenario potentiated hepatic stellate cell activation with increased expression of fibrogenic genes. HFRU20 mice showed 40% Vv [steatosis], enhanced by lipogenesis, ER stress markers, hepatic inflammation, and activated hepatic stellate cells (positive labeling for alpha-smooth muscle actin and reelin), besides perivascular fibrosis, suggesting NAFLD progression towards NASH in this dietary mouse model.

Acknowledgments

The authors would like to thank Aline de Carvalho and Andrea Bertoldo for their technical assistance.

This study was financed in part by the Coordenação de Aperfeiçoamento de Pessoal de Nível Superior - Brazil (CAPES) - Finance Code 001 (doctoral scholarships for AF-S, CSM, and FMS-V, and post-doctoral scholarship for FFM), Fundação Carlos Chagas Filho de Amparo à Pesquisa do Estado do Rio de Janeiro (Faperj – Master scholarship for BO-C). The corresponding author is supported by Conselho Nacional de Desenvolvimento Científico e Tecnológico (CNPq, grant N° 303785/2020-9, and 404446/2021-3), and FAPERJ (Grants N° E-26/200.984/2022, and E-26/010.002136/2019).

REFERENCES

- ABDELMALEK MF, SUZUKI A, GUY C, UNALP-ARIDA A, COLVIN R, JOHNSON RJ & DIEHL AM. 2010. Increased fructose consumption is associated with fibrosis severity in patients with nonalcoholic fatty liver disease. *Hepatology* 51: 1961-1971.
- AIBARA D, MATSUO K, YAMANO S & MATSUSUE K. 2020. Fat-specific protein 27b is regulated by hepatic peroxisome proliferator-activated receptor γ in hepatic steatosis. *Endocr J* 67: 37-44.
- ASGHARPOUR A ET AL. 2016. A diet-induced animal model of non-alcoholic fatty liver disease and hepatocellular cancer. *J Hepatol* 65: 579-588.
- AVRAHAMI D ET AL. 2015. Aging-Dependent Demethylation of Regulatory Elements Correlates with Chromatin State and Improved beta Cell Function. *Cell Metab* 22: 619-632.
- BRASIL. 2020. *Vigítel Brasil 2019 : vigilância de fatores de risco e proteção para doenças crônicas por inquérito telefônico : estimativas sobre frequência e distribuição sociodemográfica de fatores de risco e proteção para doenças crônicas nas capitais dos 26 estados brasileiros e no Distrito Federal em 2019 [recurso eletrônico] / Ministério da Saúde, Secretaria de Vigilância em Saúde, Departamento de Análise em Saúde e Vigilância de Doenças não Transmissíveis. – 1ª Ed. Brasília: Ministério da Saúde 2020: 137.*
- BREITKOPF K, GODOY P, CIUCLAN L, SINGER MV & DOOLEY S. 2006. TGF-beta/Smad signaling in the injured liver. *Z Gastroenterol* 44: 57-66.
- CAMELO L, MARINHO TS, AGUILA MB, SOUZA-MELLO V & BARBOSA-DA-SILVA S. 2019. Intermittent fasting exerts beneficial metabolic effects on blood pressure and cardiac structure by modulating local renin-angiotensin system in the heart of mice fed high-fat or high-fructose diets. *Nutr Res* 63: 51-62.
- CAO Y ET AL. 2022. Macrophages evoke autophagy of hepatic stellate cells to promote liver fibrosis in NAFLD mice via the PGE2/EP4 pathway. *Cell Mol Life Sci* 79: 303.
- CATTA-PRETA M, MENDONCA LS, FRAULOB-AQUINO J, AGUILA MB & MANDARIM-DE-LACERDA CA. 2011. A critical analysis of three quantitative methods of assessment of hepatic steatosis in liver biopsies. *Virchows Arch* 459: 477-485.
- CHEN N, LIU S, QIN D, GUAN D, CHEN Y, HOU C, ZHENG S, WANG L, CHEN X & ZHANG L. 2022. Fate tracking reveals differences between Reelin⁺ hepatic stellate cells (HSCs) and Desmin⁺ HSCs in activation, migration and proliferation. *Cell Prolif*: e13500.
- DE MINICIS S, DAY C & SVEGLIATI-BARONI G. 2013. From NAFLD to NASH and HCC: pathogenetic mechanisms and therapeutic insights. *Curr Pharm Des* 19: 5239-5249.
- DE OLIVEIRA SA G, DOS SANTOS NEVES V, DE OLIVEIRA FRAGA SR, SOUZA-MELLO V & BARBOSA-DA-SILVA S. 2017. High-intensity interval training has beneficial effects on cardiac remodeling through local renin-angiotensin system modulation in mice fed high-fat or high-fructose diets. *Life Sci* 189: 8-17.
- DO MH, LEE E, OH MJ, KIM Y & PARK HY. 2018. High-Glucose or -Fructose Diet Cause Changes of the Gut Microbiota and Metabolic Disorders in Mice without Body Weight Change. *Nutrients* 10: 761.
- DUNCAN MH, SINGH BM, WISE PH, CARTER G & ALAGHBAND-ZADEH J. 1995. A simple measure of insulin resistance. *Lancet* 346: 120-121.
- DUNNETT CWJOTASA. 1980. Pairwise multiple comparisons in the unequal variance case. *J Am Stat Assoc* 75: 796-800.
- FERNANDES-DA-SILVA A, MIRANDA CS, SANTANA-OLIVEIRA DA, OLIVEIRA-CORDEIRO B, RANGEL-AZEVEDO C, SILVA-VEIGA FM, MARTINS FF & SOUZA-MELLO V. 2021. Endoplasmic reticulum stress as the basis of obesity and metabolic diseases: focus on adipose tissue, liver, and pancreas. *Eur J Nutr* 60: 2949-2960.
- FERRE P & FOUFELLE F. 2010. Hepatic steatosis: a role for de novo lipogenesis and the transcription factor SREBP-1c. *Diabetes Obes Metab* 12 Suppl 2: 83-92.
- FRIEDMAN SLJPR. 2008. Hepatic stellate cells: protean, multifunctional, and enigmatic cells of the liver. *Physiol Rev* 88: 125-172.
- FUSAKIO ME, WILLY JA, WANG Y, MIREK ET, AL BAGHDADI RJ, ADAMS CM, ANTHONY TG & WEK RC. 2016. Transcription factor ATF4 directs basal and stress-induced gene expression in the

unfolded protein response and cholesterol metabolism in the liver. *Mol Biol Cell* 27: 1536-1551.

GALLIGAN JJ, SMATHERS RL, SHEARN CT, FRITZ KS, BACKOS DS, JIANG H, FRANKLIN CC, ORLICKY DJ, MACLEAN KN & PETERSEN DR. 2012. Oxidative Stress and the ER Stress Response in a Murine Model for Early-Stage Alcoholic Liver Disease. *J Toxicol* 2012: 207594.

GEORGE J, RAO KR, STERN R & CHANDRAKASAN G. 2001. Dimethylnitrosamine-induced liver injury in rats: the early deposition of collagen. *Toxicology* 156: 129-138.

GUSTAFSON B & SMITH U. 2015. Regulation of white adipogenesis and its relation to ectopic fat accumulation and cardiovascular risk. *Atherosclerosis* 241: 27-35.

HAN J & KAUFMAN RJ. 2016. The role of ER stress in lipid metabolism and lipotoxicity. *J Lipid Res* 57: 1329-1338.

HAO L ET AL. 2021. ATF4 activation promotes hepatic mitochondrial dysfunction by repressing NRF1-TFAM signalling in alcoholic steatohepatitis. *Gut* 70: 1933-1945.

HELLERBRAND C, STEFANOVIC B, GIORDANO F, BURCHARDT ER & BRENNER DA. 1999. The role of TGFbeta1 in initiating hepatic stellate cell activation in vivo. *J Hepatol* 30: 77-87.

HERMAN MA & SAMUEL VT. 2016. The Sweet Path to Metabolic Demise: Fructose and Lipid Synthesis. *Trends Endocrinol Metab* 27: 719-730.

HUMMASTI S & HOTAMISLIGIL GS. 2010. Endoplasmic reticulum stress and inflammation in obesity and diabetes. *Circ Res* 107: 579-591.

IM YR ET AL. 2021. A Systematic Review of Animal Models of NAFLD Finds High-Fat, High-Fructose Diets Most Closely Resemble Human NAFLD. *Hepatology* 74: 1884-1901.

ITO M, NAGASAWA M, HARA T, IDE T & MURAKAMI K. 2010. Differential roles of CIDEA and CIDEC in insulin-induced anti-apoptosis and lipid droplet formation in human adipocytes. *J Lipid Res* 51: 1676-1684.

JEGATHEESAN P & DE BANDT JP. 2017. Fructose and NAFLD: The Multifaceted Aspects of Fructose Metabolism. *Nutrients* 9: 230.

JIN CJ ET AL. 2020. Aging-related liver degeneration is associated with increased bacterial endotoxin and lipopolysaccharide binding protein levels. *Am J Physiol Gastrointest Liver Physiol* 318: G736-G747.

KANNT A ET AL. 2020. Incretin combination therapy for the treatment of non-alcoholic steatohepatitis. *Diabetes Obes Metab* 22: 1328-1338.

KAZANKOV K, JORGENSEN SMD, THOMSEN KL, MOLLER HJ, VILSTRUP H, GEORGE J, SCHUPPAN D & GRONBAEK H. 2019. The

role of macrophages in nonalcoholic fatty liver disease and nonalcoholic steatohepatitis. *Nat Rev Gastroenterol Hepatol* 16: 145-159.

KIEFFER TJ & HABENER JF. 2000. The adipoinsular axis: effects of leptin on pancreatic beta-cells. *Am J Physiol Endocrinol Metab* 278: E1-e14.

KIM IH, KISSELEVA T & BRENNER DA. 2015. Aging and liver disease. *Curr Opin Gastroenterol* 31: 184-191.

KOO SH. 2013. Nonalcoholic fatty liver disease: molecular mechanisms for the hepatic steatosis. *Clin Mol Hepatol* 19: 210-215.

LANASPA MA ET AL. 2018. High salt intake causes leptin resistance and obesity in mice by stimulating endogenous fructose production and metabolism. *Proc Natl Acad Sci USA* 115: 3138-3143.

LATTOUF R, YOUNES R, LUTOMSKI D, NAAMAN N, GODEAU G, SENNI K & CHANGOTADE S. 2014. Picrosirius red staining: a useful tool to appraise collagen networks in normal and pathological tissues. *J Histochem Cytochem* 62: 751-758.

LIM JS, MIETUS-SNYDER M, VALENTE A, SCHWARZ JM & LUSTIG RH. 2010. The role of fructose in the pathogenesis of NAFLD and the metabolic syndrome. *Nat Rev Gastroenterol Hepatol* 7: 251-264.

LUA I, LI Y, ZAGORY JA, WANG KS, FRENCH SW, SEVIGNY J & ASAHINA K. 2016. Characterization of hepatic stellate cells, portal fibroblasts, and mesothelial cells in normal and fibrotic livers. *J Hepatol* 64: 1137-1146.

LUSTIG RH, SCHMIDT LA & BRINDIS CD. 2012. Public health: The toxic truth about sugar. *Nature* 482: 27-29.

MACHADO MV, MICHELOTTI GA, PEREIRA TA, XIE G, PREMONT R, CORTEZ-PINTO H & DIEHL AM. 2015. Accumulation of duct cells with activated YAP parallels fibrosis progression in non-alcoholic fatty liver disease. *J Hepatol* 63: 962-970.

MAGLIANO DC, PENNA-DE-CARVALHO A, VAZQUEZ-CARRERA M, MANDARIM-DE-LACERDA CA & AGUILA MB. 2015. Short-term administration of GW501516 improves inflammatory state in white adipose tissue and liver damage in high-fructose-fed mice through modulation of the renin-angiotensin system. *Endocrine* 50: 355-367.

MANNAERTS I, LEITE SB, VERHULST S, CLAERHOUT S, EYSACKERS N, THOEN LF, HOORENS A, REYNAERT H, HALDER G & VAN GRUNSVEN LA. 2015. The Hippo pathway effector YAP controls mouse hepatic stellate cell activation. *J Hepatol* 63: 679-688.

MARTINS FF, SOUZA-MELLO V, CARVALHO JJ, DEL SOL M, AGUILA MB & MANDARIM-DE-LACERDA CA. 2021. Liver structural injury in leptin-deficient (ob/ob) mice: Lipogenesis,

fibrogenesis, inflammation and apoptosis. *Int J Morphol* 39: 732-738.

OHASHI T, KATO M, YAMASAKI A, KUWANO A, SUZUKI H, KOHJIMA M & OGAWA Y. 2018. Effects of high fructose intake on liver injury progression in high fat diet induced fatty liver disease in ovariectomized female mice. *Food Chem Toxicol* 118: 190-197.

OYADOMARI S & MORI M. 2004. Roles of CHOP/GADD153 in endoplasmic reticulum stress. *Cell Death Differ* 11: 381-389.

PAIS R, CHARLOTTE F, FEDCHUK L, BEDOSSA P, LEBRAY P, POYNARD T, RATZIU V & GROUP LS. 2013. A systematic review of follow-up biopsies reveals disease progression in patients with non-alcoholic fatty liver. *J Hepatol* 59: 550-556.

RADHAKRISHNAN S, YEUNG SF, KE JY, ANTUNES MM & PELLIZZON MA. 2021. Considerations When Choosing High-Fat, High-Fructose, and High-Cholesterol Diets to Induce Experimental Nonalcoholic Fatty Liver Disease in Laboratory Animal Models. *Curr Dev Nutr* 5: nzb138.

REEVES PG, NIELSEN FH & FAHEY JR GC. 1993. AIN-93 purified diets for laboratory rodents: final report of the American Institute of Nutrition ad hoc writing committee on the reformulation of the AIN-76A rodent diet. *J Nutr* 123: 1939-1951.

ROSA-CALDWELL ME, BROWN JL, LEE DE, WIGGS MP, PERRY RA JR, HAYNIE WS, CALDWELL AR, WASHINGTON TA, LO WJ & GREENE NP. 2020. Hepatic alterations during the development and progression of cancer cachexia. *Appl Physiol Nutr Metab* 45: 500-512.

RUTKOWSKI DT ET AL. 2008. UPR pathways combine to prevent hepatic steatosis caused by ER stress-mediated suppression of transcriptional master regulators. *Dev Cell* 15: 829-840.

SCHMIDT NH, SVENDSEN P, ALBARRAN-JUAREZ J, MOESTRUP SK & BENTZON JF. 2021. High-fructose feeding does not induce steatosis or non-alcoholic fatty liver disease in pigs. *Sci Rep* 11: 2807.

SFERRA R, VETUSCHI A, POMPILI S, GAUDIO E, SPECA S & LATELLA G. 2017. Expression of pro-fibrotic and anti-fibrotic molecules in dimethylnitrosamine-induced hepatic fibrosis. *Pathol Res Pract* 213: 58-65.

SHIBATA Y, VOELTZ GK & RAPOPORT TA. 2006. Rough sheets and smooth tubules. *Cell* 126: 435-439.

SILVA-VEIGA FM, MIRANDA CS, MARTINS FF, DALEPRANE JB, MANDARIM-DE-LACERDA CA & SOUZA-MELLO V. 2020. Gut-liver axis modulation in fructose-fed mice: a role for PPAR-alpha and linagliptin. *J Endocrinol* 247: 11-24.

SMITH-CORTINEZ N ET AL. 2021. Collagen release by human hepatic stellate cells requires vitamin C and is efficiently blocked by hydroxylase inhibition. *FASEB J* 35: e21219.

STAHL EC ET AL. 2020. Inflammation and Ectopic Fat Deposition in the Aging Murine Liver Is Influenced by CCR2. *Am J Pathol* 190: 372-387.

TAPPY L & JEQUIER E. 1993. Fructose and dietary thermogenesis. *The American journal of clinical nutrition* 58: 766S-770S.

TIAN J & LOCKER J. 2013. Gadd45 in the liver: signal transduction and transcriptional mechanisms. *Adv Exp Med Biol* 793: 69-80.

TSCHANZ SA, BURRI PH & WEIBEL ER. 2011. A simple tool for stereological assessment of digital images: the STEPanizer. *J Microsc* 243: 47-59.

URTASUN R, CUBERO FJ & NIETO N. 2012. Oxidative stress modulates KLF6Full and its splice variants. *Alcohol Clin Exp Res* 36: 1851-1862.

VASQUES-MONTEIRO IML, SILVA-VEIGA FM, MIRANDA CS, DE ANDRADE GONCALVES ECB, DALEPRANE JB & SOUZA-MELLO V. 2021. A rise in Proteobacteria is an indicator of gut-liver axis-mediated nonalcoholic fatty liver disease in high-fructose-fed adult mice. *Nutr Res* 91: 26-35.

WANG Y, ZHANG L, WU X, GURLEY EC, KENNEDY E, HYLEMON PB, PANDAK WM, SANYAL AJ & ZHOU H. 2013. The role of CCAAT enhancer-binding protein homologous protein in human immunodeficiency virus protease-inhibitor-induced hepatic lipotoxicity in mice. *Hepatology* 57: 1005-1016.

WIRTH A, WANG S, TAKEFUJI M, TANG C, ALTHOFF TF, SCHWEDA F, WETTSCHURECK N & OFFERMANN S. 2016. Age-dependent blood pressure elevation is due to increased vascular smooth muscle tone mediated by G-protein signalling. *Cardiovasc Res* 109: 131-140.

WOUTERS K ET AL. 2008. Dietary cholesterol, rather than liver steatosis, leads to hepatic inflammation in hyperlipidemic mouse models of nonalcoholic steatohepatitis. *Hepatology* 48: 474-486.

XIAO G, ZHANG T, YU S, LEE S, CALABUIG-NAVARRO V, YAMAUCHI J, RINGQUIST S & DONG HH. 2013. ATF4 protein deficiency protects against high fructose-induced hypertriglyceridemia in mice. *J Biol Chem* 288: 25350-25361.

YANG Y, KIM B, PARK YK, KOO SI & LEE JY. 2015. Astaxanthin prevents TGFbeta1-induced pro-fibrogenic gene expression by inhibiting Smad3 activation in hepatic stellate cells. *Biochim Biophys Acta* 1850: 178-185.

ZHANG DM, JIAO RQ & KONG LD. 2017. High Dietary Fructose: Direct or Indirect Dangerous Factors Disturbing Tissue and Organ Functions. *Nutrients* 9: 335.

ZHAO Y, WANG QY, ZENG LT, WANG JJ, LIU Z, FAN GQ, LI J & CAI JP. 2022. Long-Term High-Fat High-Fructose Diet Induces Type 2 Diabetes in Rats through Oxidative Stress. *Nutrients* 14: 2181.

SUPPLEMENTARY MATERIAL

Table S1.

How to cite

OLIVEIRA-CORDEIRO B, FERNANDES-DA-SILVA A, SILVA-VEIGA FM, MIRANDA CS, MARTINS FF & SOUZA-MELLO V. 2023. Long-term hepatic damage in high-fructose-fed C57BL/6 mice: hepatic fibrogenesis, endoplasmic reticulum stress markers, and fibrosis. *An Acad Bras Cienc* 95: e20220784. DOI 10.1590/0001-3765202320220784.

*Manuscript received on September 10, 2022;
accepted for publication on April 19, 2023*

BRENDA OLIVEIRA-CORDEIRO*

<https://orcid.org/0009-0007-1407-5918>

ALINE FERNANDES-DA-SILVA*

<https://orcid.org/0000-0002-6369-0235>

FLAVIA MARIA SILVA-VEIGA

<https://orcid.org/0000-0002-3320-5825>

CAROLLINE S. MIRANDA

<https://orcid.org/0000-0001-5488-0179>

FABIANE F. MARTINS

<https://orcid.org/0000-0002-3831-6604>

VANESSA SOUZA-MELLO

<https://orcid.org/0000-0002-2510-9569>¹

Universidade do Estado do Rio de Janeiro, Instituto de Biologia Roberto Alcântara Gomes, Laboratório de Morfometria, Metabolismo e Doenças Cardiovasculares, Boulevard 28 de Setembro, 87, fundos (andar térreo), Vila Isabel, 20551-030 Rio de Janeiro, RJ, Brazil

Correspondence to: **Vanessa Souza-Mello**

E-mail: souzamello.uerj@gmail.com

*These authors contributed equally to the manuscript.

Author contributions

B.O.-C. and A.F.-S.: Generation, collection, assembly, analysis, and interpretation of data, manuscript draft; F.M.S.-V., C.S.M.: Generation, collection, assembly, analysis, and interpretation of data; F.F.M.: Analysis and interpretation of data, revision of the manuscript; V.S.-M.: Conception and design of the study, analysis and interpretation of data, revision of the manuscript, supervision.

